

# Merging of globular clusters within inner galactic regions. I. Do they survive the tidal interaction?

P. Miocchi

miocchi@uniroma1.it

R. Capuzzo Dolcetta

dolcetta@uniroma1.it

P. Di Matteo

p.dimatteo@uniroma1.it

and

A. Vicari

alessandrovicari@uniroma1.it

*Dipartimento di Fisica, Università di Roma “La Sapienza”,  
P.le Aldo Moro, 2, I00185 – Rome, Italy.*

## ABSTRACT

The main topic of this paper is the investigation of the modes of interaction of globular clusters (GCs) moving in the inner part of a galaxy. This is tackled by means of high-resolution  $N$ -body simulations, whose first results are presented in this article. Our simulations dealt with primordial very massive (order of  $10^7 M_{\odot}$ ) GCs that were able to decay, because of dynamical friction, into the inner regions of triaxial galaxies on a time much shorter than their internal relaxation time. To check the disruptive roles of both tidal forces and GC-GC collisions, their effects were maximised by considering clusters on quasi-radial orbits and choosing the initial conditions so as to give head-on collisions at each passage through the center.

The available CPU resources allowed us to simulate clusters with different structural parameters and to follow them on quasi-radial orbits during 8 passages across the center. The main findings are: i) clusters with an initial high enough King concentration parameter ( $c \geq 1.2$ ), preserve up to 50% of their initial mass; ii) the inner density distribution of the survived clusters keep a King model profile; iii) GC-GC collisions have a negligible effect with respect to that caused by the passage through the galactic center; iv) the orbital energy dissipation due to the tidal interaction is of the same order of that caused by dynamical friction; v) complex sub-structures like “ripples” and “clumps” formed, as observed around real clusters. These findings support the validity of the hypothesis of merging of GCs in the galactic central region, with modes that deserve further careful investigations.

*Subject headings:* globular clusters: general, galaxies: kinematics and dynamics, methods: N-body simulations

## 1. Introduction

The study of the detailed structure and evolution of globular clusters (GCs) in galaxies is a modern astrophysical concern, which is particularly suitable for HST (Kundu et al. 1999) and for large ground-based telescopes (Gomez et al. 2001). Some interesting general considerations on the structural properties of GCSs in galaxies are found in Ashman & Zepf (1997), where also a summary of simplified models and results by other authors on the topic of formation and destruction of globular clusters in galaxies is present. While the amount of data for GCSs in galaxies is now large and rapidly increasing (see, e.g. Davidge & van den Bergh 2005; Dirsch et al. 2005; Forbes et al. 2004; Fort et al. 1986; Gomez & Richtler 2004; Kundu et al. 2004; Olsen et al. 2004; Zepf et al. 2004), from a theoretical point of view the study of the evolution of GCSs in galaxies has been tackled in different ways but it still lacks of definitive conclusions. We just recall here the studies by Aguilar et al. (1988), Gnedin & Ostriker (1997) and Vesperini (2001), which aim at achieving a deeper understanding of the effects of the interaction of clusters with the galactic field, and the interesting results obtained by Gnedin et al. (1999) on the survival of clusters in dependence on their initial conditions.

It is known that, in elliptical galaxies, the most important processes causing the evolution of GCs are i) the tidal interaction with the global field (Murali & Weinberg 1997a), that has also ii) the effect of accelerating the relaxation evaporation (Murali & Weinberg 1997b); iii) the impulsive interaction with a compact object in the galactic center (on much smaller length-scales), see Ostriker et al. (1989), Capuzzo Dolcetta (1993), Capuzzo Dolcetta & Tesseri (1997), Capuzzo Dolcetta & Tesseri (1999); iv) the dynamical friction (df) due to the bulge-halo matter as firstly shown by Tremaine et al. (1975) and then generalised to the triaxial galaxies case by Pesce et al. (1992), Capuzzo Dolcetta (1993), Capuzzo Dolcetta & Vicari (2005), who ascertained that df plays a much more important role than what previously believed; see also Colpi et al. (1999), van den Bosch et al. (1999), Peñarrubia et al. (2002).

Actually, Pesce et al. (1992) (hereafter PCV), Capuzzo Dolcetta (1993) and Capuzzo Dolcetta

& Vicari (2005) showed quantitatively (by mean of numerical integration of a large set of orbits of GCs in self-consistent galactic models) that massive enough clusters have short orbital decaying times. More specifically, Eqs. (A1) and (A2) in Capuzzo Dolcetta (1993) indicate the (almost) total loss of the orbital energy in less than 5 Gyr for  $10^6 M_{\odot}$  GCs on low angular momentum orbits having an initial orbital binding energy per unit mass  $E = 0.6$ , which is (in units of the galactic total potential depth) the energy corresponding to the background stellar velocity dispersion in the assumed Schwarzschild's triaxial model (Schwarzschild 1979); this decay time, inversely scaling with GC mass, is less than 500 Myr for globulars more massive than  $10^7 M_{\odot}$ . Incidentally, the apocentric distance of a quasi-radial orbit (thin box) of  $E = 0.6$  is  $6.3r_b$  while the radius of the quasi-circular orbit of same energy is  $3.8r_b$ , where  $r_b$  is the core radius of the Schwarzschild's (1979) model spherical component; the assumption (as in Schwarzschild 1979)  $r_b = 200$  pc gives 1.3 kpc and 760 pc for the apocenter and circular radius, respectively. The more recent paper Capuzzo Dolcetta & Vicari (2005) represents a generalization and widening of the previous PCV and Capuzzo Dolcetta (1993) works and refers to a set of model for triaxial galaxies with a density core and various axial ratios. For the sake of comparison with the above cited results based on the Schwarzschild's model, a semimajor axis of 300 pc and the same axial ratios 2:1.25:1 of that model are used in the df decay time fitting formulas given in Capuzzo Dolcetta & Vicari (2005) to get, for the same  $10^6 M_{\odot}$  GC of the same initial orbital energy and angular momentum, a decay time  $10^9$  yr, i.e. a factor 5 shorter than the one evaluated as described above. Being the df time easily evaluated for any GC mass, due to its inverse proportionality to the mass, we get a decay time ranging from  $10^8$  yr to 20 Gyr for an interval of GC masses extending from  $5 \times 10^4 M_{\odot}$  to  $10^7 M_{\odot}$ , implying a significant evolution of an initial GC population by df, as actually shown by Capuzzo Dolcetta & Vicari (2005).

One application of the present work is to the study of the validity of an intriguing scenario elsewhere presented (Capuzzo Dolcetta 1993) and that naturally emerges from all these considerations: the high efficiency of the df implies that

many massive ( $M \gtrsim 5 \times 10^6 M_\odot$ ) globular clusters decay rapidly to the inner galactic region where they interact closely with each other and with the galactic nucleus, eventually forming, through a merging process, a dense and massive super-cluster. This scenario, that requires an accurate modeling, has important implications both on the accretion of massive objects in the galactic center and on their radiative emission as AGN (see the discussion in Capuzzo Dolcetta 1993; Capuzzo Dolcetta & Vicari 2005).

One crucial point for this scheme to work is the existence of few primordial massive GCs. At this regard, we remind that the real problem was, once, to understand why very massive GCs were not observed, indeed. This because the typical Jeans mass in a primordial, virialized, gaseous galactic halo ( $T \simeq 10^5 \div 10^6$  K) is  $> 10^7 M_\odot$ , which is too large respect to the observed (Milky Way) GC mass values. This led to the theoretical attempt to understand why such massive GCs were not observed, on the basis of various schemes and scenarios of GC formation (Fall & Rees (1985), Vietri & Pesce (1995)) mainly invoking the efficiency of cooling mechanisms reducing the temperature to low enough values. The new, relevant, point is that there are now quite a few recent papers showing, indeed, the existence of *young* massive clusters in Antennae (Fritze-v. Alvensleben 1999), in the Magellanic Clouds, M33, Fornax dSph (de Grijs et al. 2005). Young massive clusters have been found, also, in M31 (Fusi Pecci et al. 2005); in this galaxy, Huxor et al. (2005) discovered bright clusters with anomalously large half-mass radii ( $\approx 30$  pc).

In particular, Fritze-v. Alvensleben (1999) showed that the mass function of young clusters in the Antennae extends up to few times  $10^7 M_\odot$ . The existence of very massive GCs does not seem to be a peculiarity of young systems, only. Actually, Harris & Pudritz (1994) give the evidence of the presence of  $10^7 M_\odot$  in the giant elliptical M87 as well as in Virgo ellipticals, being the cumulative (sum over 3 ellipticals in the cluster) mass function of GCs extended up to high masses. The observed presence of very massive GCs fits with the recent theoretical-numerical findings by Kravtsov & Gnedin (2005) who deduce a dependence of the most massive GC mass ( $M_{max}$ ) on the parent galaxy mass ( $M_g$ ),  $M_{max} \propto M_g^{1.29}$ ,

such that  $M_{max} \simeq 10^7 M_\odot$  for  $M_g \simeq 2.6 \times 10^{11} M_\odot$ . Moreover, they also find that very massive GCs contribute to more than 50% to the total cluster mass, in fine agreement with the observational data of Harris et al. (2006) that indicate how up a full 40% of the total mass that is now in the GCSs of brightest cluster galaxies is contributed by massive (present day mass  $> 1.5 \times 10^6 M_\odot$ ). It may be also worth remembered the specific paper by Baumgardt et al. (2003) devoted to the modeling of G1, the massive GC in M31, obtaining for it a mass  $8 \times 10^6 M_\odot$ .

Consequently, one can just make a hypothesis on the initial abundance of massive clusters and see whether it gives results consistent with available observations, checking, of course the dependence of results on the assumption. This was done in Capuzzo Dolcetta & Vicari (2005), that shows (see their Fig.11) how few tens of massive ( $M > 10^7 M_\odot$ ) clusters suffice to give an accretion rate onto a central galactic black hole high enough (few  $M_\odot \text{ yr}^{-1}$ ) to sustain an AGN activity. Given all this, our main concern is to check whether or not the tidal distortion suffered by the GCs due to the halo and the bulge is destructive on the time-scale needed by df to dissipate the cluster orbital energy. The detailed numerical studies performed by Charlton & Laguna (1995); Nordquist et al. (1999) give encouraging support to this claiming. In this paper, we show the results of detailed  $N$ -body simulations that take into account df and two other concurrent effects: i) the tidal interaction of a GC with the overall galactic field and ii) the collision with another passing-by GC. We consider quasi-radial orbits for GCs, such to maximise the tidal effects.

As a ‘by-product’ of this work, tidal tail formation and morphology is analysed and a particular attention is focused on the presence of overdensities (clumps) in the tails. Similar sub-structures have been detected in the two tidal tails of the globular cluster Palomar 5 (Odenkirchen et al. 2001, 2003), while the presence of tails surrounding many other GCs is strongly suggested by various observations (Lehmann & Scholz 1997; Testa et al. 2000; Leon et al. 2000; Siegel et al. 2001; Lee et al. 2003). NGC 6254 and Palomar 12 seem to show similar overdensities in their tails, too (Leon et al. 2000). Various authors attribute the formation of clumps in the tails to strong gravitational

shocks suffered by the cluster (Combes et al. 1999) and, in particular, to the tidal effect due to compact galactic sub-structures (Dehnen et al. 2004), like molecular clouds or spiral arms. Nevertheless, the mechanisms of their origin and formation is still unclear and deserve an adequate interpretation. More recently, Capuzzo Dolcetta, Di Matteo & Miocchi (2005) (hereafter CDM) showed that clumpy tails emerge also in GCs moving in a regular ‘smooth’ galactic environment on both quasi-circular and more eccentric orbits, suggesting that such clumpy sub-structures are related to the local decrease of the stars velocity along the tails (see also Di Matteo, Capuzzo Dolcetta & Miocchi, 2005).

This paper is organized as follows: in Sect.2 the numerical modeling is described, the results are shown and discussed in Sect.3 and conclusions drawn in Sect.4.

## 2. The model

We consider GCs as  $N$ -body systems moving within a triaxial galaxy represented by an analytical potential (see next Section), including the deceleration due to dynamical friction caused by the field stars. We studied the evolution of a pair of GCs whose center-of-mass (CM) initial conditions were assigned such to put them along very elongated orbits. They start moving on opposite sides respect to the galactic center and oscillate quasi-radially around it, crossing and colliding each other in the galactic center neighbourhood (see, e.g., the upper panel in Fig. 3). Both the choice of very elongated orbits and the presence of two clusters were motivated by the wish to study the combined effects of the tidal interaction and of the collisions between GCs. Indeed, when such systems undergo the final stages of orbital decay, GC-GC merging and close interactions are expected to occur.

We dealt with four different types of clusters, named (a) , (b) , (c) and (d) at increasing order of concentration (see Table 1 and Sect.2.2). Their dynamics was modelled in simulation A, that involved the pair of clusters (a) and (b) , and in simulation B that regarded the more compact clusters (c) and (d) . We also considered a further case (simulation C) where the dynamics of cluster (a) , with the same initial conditions as in simulation

A, was followed *without* the presence of the other cluster. This latter simulation lasted less than the others due to CPU-time limitations. Note that the total CPU-time spent by all the simulations presented here is about 30,000 hours divided among the 64 processors used on an IBM SP4 system (granted by the INAF-CINECA agreement).

In this paper, unless otherwise specified, lengths, masses and time are measured, respectively, in unit of the galactic core radius  $r_b$ , of the galactic core mass  $M_b$  and of the galactic core crossing time  $t_b = (r_b^3/GM_b)^{1/2}$ . Note that the numerical values in physical units of the mentioned parameters are irrelevant for the results of the simulations, that can be always scaled as long as the ratios  $t/t_b$ ,  $r/r_b$ ,  $M/M_b$  (with  $M$  the total cluster mass) are kept unchanged. This is strictly true only if one can neglect, like in our case, the effects due to 2-body stellar collisions (as discussed in Sect.2.2), otherwise the dynamics would depend also on the mass of the *single* star in the clusters.

The reference frame was fixed with the origin at the galactic center and the  $x$  and  $z$  axes, respectively, along the maximum and minimum axis of the triaxial ellipsoid. The cluster CM was initially located on the  $x$ -axis: cluster (a) and (c) at  $x_0 = -4.15$ , and cluster (b) and (d) at  $x_0 = 3.95$ . In all the cases the initial velocity components were (0, 0.05, 0.025). Because of the CPU time limitations, we were not able to consider a wide set of initial conditions, thus we decided to choose initial velocity and position in such a way as to set *upper* limits to the disruptive effects exerted on massive clusters by the tidal interaction with the galactic field and by the close interaction with other GCs. For this reason, we chose almost radial orbits so that the GCs cross twice per period the galactic center, where the tidal interaction is strongest, and they undergo head-on collisions with each other while crossing the center.

Moreover, the range of initial orbital parameters compatible with our assumed starting conditions obviously depends on the actual age of simulated clusters, that cannot be univoquely defined (clusters of different ages and different initial conditions may have the same apocenter and velocity we chose to start simulations). However, we checked that in the adopted triaxial potential all GCs with masses in the range  $(1.5-2.0) \times 10^7 M_\odot$  (see Section 2.2 and Table 1) and moving on either

box orbits or loop orbits with pericenter  $\simeq 0$  and initial apocenter in the interval 3.5–4 kpc decay (due to dynamical friction) to our starting conditions in about 1 Gyr (having set  $M_b = 3 \times 10^9 M_\odot$  and  $r_b = 200$  pc). The decay time can be easily scaled to any GC mass, due to its inverse linear proportionality to it, that means a decay time 2 Gyr for a GC half that massive.

As regards the computational techniques, we adopted a direct  $N$ -body representations for the stars in the clusters, simulating their dynamics by mean of the parallel MPI ‘ATD’ code (Miocchi & Capuzzo Dolcetta 2002) whose main features are resumed in Appendix B.

## 2.1. The galactic model

We considered the same self-consistent triaxial model described in de Zeeuw & Merritt (1983) and in PCV; the same model was also used in CDM to study tidal tails formation around clusters in absence of df and on not very elongated orbits. It corresponds to a non-rotating ellipsoidal, triaxial distribution of matter with axial ratios 2:1.25:1 (Schwarzschild, 1979), which leads to a projected profile in agreement with that observed in spirals spheroids (see, e.g., Bertola et al. 1991; Matthews & de Grijs 2004) and in elliptical galaxies (see, e.g., Wagner 1988; Davies et al. 2001; Statler et al. 2004). The potential produced can be expressed as the sum of a spherically symmetric term due to a density following the modified Hubble’s law

$$\rho_b(r) = \rho_{b0} \left[ 1 + \left( \frac{r}{r_b} \right)^2 \right]^{-3/2}, \quad (1)$$

with  $r_b$  the core radius and  $\rho_{b0} = M_b/r_b^3$ , plus other two non-spherical terms that give the triaxial behaviour, i.e.

$$\Phi(x, y, z) = A[\Phi_r(r) + \Phi_1(z, r) + \Phi_2(x, y, r)], \quad (2)$$

with  $A \equiv 4\pi GM_b$  and

$$\Phi_r = -\frac{1}{r} \ln \left( \frac{r}{r_b} + \sqrt{1 + \left( \frac{r}{r_b} \right)^2} \right), \quad (3)$$

$$\Phi_1 = c_1 \frac{3z^2 - r^2}{2(r_b^2 + c_2 r^2)^{3/2}}, \quad (4)$$

$$\Phi_2 = -3c_3 \frac{x^2 - y^2}{(r_b^2 + c_4 r^2)^{3/2}}, \quad (5)$$

The coefficients  $c_i$  have been chosen in such a way to have density axial ratios roughly constant with  $r$  (de Zeeuw & Merritt 1983), i.e.:  $c_1 = 0.06408$ ,  $c_2 = 0.65456$ ,  $c_3 = 0.01533$ ,  $c_4 = 0.48067$ . We refer to the parameter  $M_b$  as the galaxy mass, though this model yields a total infinite mass. Actually,  $M_b \simeq 0.45M(r_b)$  being  $M(r_b)$  the mass enclosed in the sphere with radius  $r_b$ . The force produced by the galactic potential is evaluated analytically and then added to each particle acceleration during the simulations.

With regard to the df, we used the generalization of the Chandrasekhar formula (Chandrasekhar 1943) to the triaxial case (PCV), with a self-consistent evaluation of the velocity dispersion tensor, taking also into account that the GC is an extended object (see Appendix A for details). We checked the dependence of df decay on applying it to the center of mass of the GC and to its center of density (see Sect. 3.2).

## 2.2. The cluster model

Our  $N$ -body simulations involved four different clusters. They sample a King distribution, with  $M$  the total mass,  $\sigma$  the central velocity dispersion,  $r_t$  and  $r_c$ , the limiting and the King radius respectively,  $c = \log(r_t/r_c)$  the concentration parameter and, finally,  $t_c = (r_c^3/GM)^{1/2}$  the core-crossing time. The ‘limiting radius’ is the radius at which the King distribution function drops to zero to model the presence of the external field (King 1966). Of course, for consistency, the limiting radius should be of the same order of the tidal radius corresponding to the local tidal field. Anyway, in order to model the presence of some tidal debris around the clusters since the initial time, the limiting radius was chosen to be 20–60% larger than the maximum tidal radius. This maximum value is achieved at the apocenter, i.e. at the initial cluster position, where it can be estimated as  $r_0(M/M(r_0))^{1/3} \simeq 0.3$  (being  $r_0 \simeq 4$  and  $M(r_0) \simeq 14$ ). However, the amount of cluster mass lying outside the tidal radius is in any case less than about 1% of the total mass. The initial values of the parameters are listed in Table 1.

Each cluster was represented with  $N = 5 \times 10^5$  ‘particles’ in the numerical model. The particles were assigned a mass according to a Salpeter’s mass distribution ( $dN/dm \propto m^{-2.35}$ ) in the range  $3.3 \times 10^{-11} \div 3.3 \times 10^{-9}$  (if, e.g.,  $M_b = 3 \times 10^9 M_\odot$

then this range is  $0.1 \div 10 M_{\odot}$ ) then, all the particle masses were uniformly re-scaled such to give the desired  $M$ . The choice to represent the GC with the ‘right’ value for the total mass, thus overestimating the individual star masses for a factor  $N_{true}/N$ , where  $N_{true}$  is the real number of stars in the GC, is the same done by, e.g., Combes et al. (1999). Anyway, both the relative stellar abundances and the total binding energy are correctly reproduced, thus we expect that the representation of the external tidal effects on the internal velocity distribution (which actually drives mass loss from the cluster) is correct as long as the spurious heating effect introduced by the overestimate of stellar masses is not relevant. As a matter of fact, we checked (see later in this Sect. and Sect. 3.1.3) that this heating is absolutely negligible over the time length of our simulations.

There are, of course, other possibilities to pick particle masses. For example, Ideta & Makino (2004) and Dehnen et al. (2004) assume all particles to have the same mass. This corresponds to an individual mass of about  $130 M_{\odot}$  in the case of the simulations of the formation of the massive  $\omega$  Cen cluster (Ideta & Makino 2004), and of about  $1 M_{\odot}$  in the case of the study of tidal tail formation around the light Pal 5 cluster. Another possible choice is that of having particle masses distributed according to an assumed stellar mass function, subsequently rescaling other relevant GC characteristic parameters (as done by, e.g., Baumgardt & Makino (2003)).

All these choices have critical aspects, unavoidably due to the limited number of particles allowed. In particular, as said above, our choice may imply spurious heating effects (as shown in the context of numerical galaxy formation by Steinmetz & White (1997)), in what fluctuations over the mean field are enhanced by the too high ‘star’ mass value. However, fluctuations should not be exceedingly important because the total mass of the system (the most relevant parameter in determining the GC mean field) is kept at its right value. In this respect, note that the half-mass relaxation time  $t_{rh}$  can be evaluated as (Spitzer 1987):

$$\frac{t_{rh}}{t_b} = \frac{t_c}{t_b} \times \frac{N}{7 \ln \Lambda}, \quad (6)$$

where, e.g. for the most compact cluster (d),  $t_c/t_b \sim 3.7 \times 10^{-2}$  (Table 1). Following Giersz &

Heggie (1994),  $\Lambda \simeq 0.1N$ , thus the above written formula gives  $t_{rh} \sim 240t_b$  for the system (d) in the numerical model. Since our simulations reached about  $40t_b$ , we can say that ‘spurious’ collisional effects should be always negligible. We say ‘spurious’ because, of course, such effects are even more negligible for the ‘real’, physical, clusters. Indeed, if, say,  $M_b = 3 \times 10^9 M_{\odot}$ , then cluster (a), for instance, would have  $M = 2 \times 10^7 M_{\odot}$ ; hence, if the stellar average mass is  $\langle m \rangle \simeq 0.3 M_{\odot}$ , it would be made up of  $N = 7 \times 10^7$  stars, making the real relaxation time even longer than the simulated time. Finally, our simulations start with clusters that have an age less than their internal 2-body relaxation time, so we assumed no initial mass segregation.

In Fig. 1 the orbits of the most concentrated clusters, (c) and (d) are plotted, as turned out from simulation B (for which clusters keep always a well defined core). They are quite elongated box orbits and represent the motion of the cluster *center-of-density* (CD), i.e. the average of the particles positions weighted with the local density instead of the mass (Casertano & Hut 1985). In most cases, we decided to take the CD as the best suitable reference for that regards the study of the internal cluster properties. Indeed, as we verified, the CM position is strongly influenced by the very extended tidal tails which quickly formed, so to be located even well outside the clusters’ core.

### 3. Results

#### 3.1. The effects of the tidal shock on the GCs internal structure

##### 3.1.1. The clusters internal ‘heating’

In Figs 2 and 3, for each cluster we plot the total internal kinetic energy ( $K$ ) and the internal gravitational potential energy ( $U$ ) of that part of the cluster that is enclosed in the sphere centered at the CD with a radius equal to the initial King radius of the cluster itself. ‘Internal’ means that  $K$  is evaluated with respect to the cluster CM, while in  $U$  the ‘external’ potential produced by the galaxy and by the other cluster is not taken into account. Considering the least compact clusters, (a) and (b), one can note, from Fig. 2, that the potential energy drops off (whereas  $K$  shows an ‘impulse’) when the clusters pass across the *core*

of the galaxy, in agreement with the fact that their inner part undergoes a violent compression at that moment, as clearly confirmed by Fig. 4. Afterwards, the potential energy seems to recover its previous level, but not completely because after each core-crossing a certain amount of potential energy is irreversibly lost by the clusters, in favour of some internal ‘heating’. All this is true especially for the least compact clusters (a) and (b), while (c) and (d) models suffer this tidal influence in their external regions only. Note, indeed, the much smaller variations in  $U$  and  $K$  (Fig. 3) and the nearly constant Lagrangian radius of 10% of the mass (Fig. 4) for the most concentrated clusters.

The energy input is due to the tidal interaction with the environment and not to the direct collision between the two clusters, as verified by a careful comparison of the time behaviour of the  $x$  coordinate of the CDs and of the energy (Figs 2 and 3). This is confirmed by the results of the simulation C that involves the presence of the cluster (a) *alone*, thus excluding any effect due to GC-GC collision. It can be affirmed that, at least within the simulated time, both the energy behaviour and the motion of the cluster show no appreciable difference when it is alone in comparison with the case when it is in a pair.

Such a conclusion is not that surprising for orbits, like those investigated here, that give rise to collisions with a high relative velocity  $V$  ( $V/\sigma \sim 60$ , being  $\sigma \sim 0.1$  the cluster internal velocity dispersion). Notice, indeed, that the duration of a head-on collision is  $\sim r_c/V \sim 10^{-2}$  which is shorter than the crossing time of our simulated clusters, so that the ‘impulse approximation’ can be applied in order to estimate the change in the clusters energy (per unit mass),  $E = U + K$ , due to *one* collision, that is (Binney & Tremaine 1987):  $\Delta E \sim G^2 M^2 (V^2 r_c^2)^{-1} \sim \sigma^4 V^{-2} \sim |E|(\sigma/V)^2$ . Hence the number of collisions needed to change appreciably the internal energy of the clusters is of order of  $|E|/\Delta E \sim (V/\sigma)^2 \sim 10^3$ , i.e. much more than that occurred in our simulated time. Of course, for smaller  $V$  such an approximation is no longer valid and the close encounters may contribute furtherly to enhance the probability of merging between clusters, as suggested by the simulations of superclusters merging in Fellhauer & Kroupa (2002) and discussed in detail in a forth-

coming paper.

Note that while the loosest clusters (a) and (b) appear almost destroyed at  $t \gtrsim 10$ , when  $E \gtrsim 0$  and the CD oscillation around the galactic center begins to lose its regularity (see Fig. 2), the more compact clusters in the simulation B are able to survive the tidal stress (Fig. 3).

### 3.1.2. The mass loss

The mass loss of the simulated GCs is due to the tidal interaction with the galactic potential. Indeed, we checked that the same cluster models used in the simulations if evolved at rest and without any external field for a time equal to the time of the simulations, exhibit a mass loss rate (in terms of particles escaping out of the limiting radius) not greater than 1%, presumably due to the (small) relaxation effects.

We quantify the amount of the mass lost adopting various criteria. According to an ‘energetic’ one,  $\mu_E$  is the fraction of the mass lost made up of the stars whose internal energy —i.e. that due only to the other stars of the same GC and evaluated in the reference frame with the origin at the cluster CD— is non-negative. This criterion is not rigorous because the sign of the individual star energy does not guarantee its ‘dynamical destiny’. Another indication of the mass lost from the clusters may be given with reference to observations. Defining as ‘lost’ those stars that belong to regions where the local GC density falls below  $\alpha \rho_b$ , the choices of  $\alpha = 1$  and  $\alpha = 0.1$  lead to the quantities  $\mu_1$  and  $\mu_{0.1}$  as fractions (to the total initial “observable” GC mass) of mass lost from the GC reported in Fig. 5.

Note that all the escaping criteria give very similar behaviours, especially for the most compact clusters. This behaviour is well fitted by a law of the form  $\mu \sim 1 - a \exp(-t/\tau)$ ; in Table 2 the best-fit parameters are given for the various GCs according to the different criteria adopted. Note, also, that although the initial limiting radii are greater than the local tidal radius, the cluster mass initially outside the tidal radius is, in any model, less than the 1% of the total mass, giving a negligible contribution to the overall mass loss.

Even if the statistics is poor (only 4 models), nevertheless we quantified a correlation between the King concentration parameter  $c$  and

$\tau_E$  (the Pearson’s linear correlation coefficient between  $\ln \tau_E$  and  $\ln c$  is 0.992). The best power law correlation in the bi-logarithmic plane (least  $\chi^2$  fit, corresponding to  $\chi^2 = 0.091$ ) is  $\tau_E/t_b \simeq 14 \times c^{6.1}$ .

### 3.1.3. Density profiles and mass segregation

For the two most compact clusters ((c) and (d)) in the simulation B, we were able to fit the inner radial density profile with a King distribution throughout the whole simulated time, as shown in Figs 6–7. We also studied the time behaviour of the concentration parameter ( $c$ ), of the central velocity dispersion ( $\sigma$ ) and of the limiting ( $r_t$ ) and King ( $r_c$ ) radii for both clusters (Fig. 8). Four points are of particular interest: i) the GCs remain bound and keep a well defined spherical “core”; ii) the inner part of the clusters tends towards less and less concentrations (see also the bottom panel of Fig. 5); iii)  $c$  shows wide oscillations coinciding, temporally, with the repeated compressions and re-expansions experienced by the clusters at each passage in the galactic core (see Fig. 4); iv)  $\sigma$  appears to be roughly constant. The decrease of the concentration is due to both the growth of the King radius and to the decrease of the limiting radius. The former is caused by the continuous re-virialization of the core as the cluster loses mass, while the latter is a direct consequence of the tidal erosion occurring preferentially in the system outskirts.

It is worth noting that in our case the tidal erosion is strong enough to act much more rapidly than 2-body collisions ( $\tau \lesssim t_{rh}/10$ ). This explains the apparent contradiction of our results, in particular point (ii), with those of other authors investigating the role of tidal interaction, e.g. Gnedin et al. (1999). Indeed, they found, by means of Fokker-Planck simulations of a GC undergoing tidal forces much weaker than in our case, that the tidal erosion acts just to accelerate the core collapse on its characteristic time scale, which is of the order of tens of  $t_{rh}$ . At this same regard, we note that an initial growth of the core of not too concentrated clusters was already found by Spitzer & Chevalier (1973) and Spitzer & Shull (1975) (in the cases of single-mass and multimass Montecarlo models, respectively) on a time scale short compared to  $t_{rh}$ , followed by a rapid evaporation-induced core collapse.

In order to investigate possible mass segrega-

tion phenomena —not expected to be relevant because the simulated time is short in comparison with the 2-body relaxation time— we analysed the evolution of the average mass of stars within three different clusters regions in simulation B: only for cluster (c) in the pair, a rather small increase of the average mass is found ( $\sim 10\%$  of the initial value) in the inner part, i.e. in the sphere where the cluster included initially 20% of its mass. In the outskirts and in the tails no appreciable mass segregation occurs. This confirms the absence of significant collisional effects that, if present, would have indicated either an influence of the external tidal field in decreasing the relaxation time, or a too small number of particles with respect to the actual number of stars.

### 3.2. The orbital decay

In the framework of our main scientific motivation, it is important to quantify how fast GCs decay towards the center of their parent galaxy. At this purpose we defined the adimensional quantity

$$\xi_{orb}(t) = \frac{E_{orb}(t) - \Psi_0}{E_0 - \Psi_0}, \quad (7)$$

where  $E_{orb}$  is the orbital energy of the CD of the cluster,  $E_0 = E_{orb}(0)$  and  $\Psi_0 = -4\pi GM_b/r_b$  is the galactic potential well. If neither dissipation nor ‘energy injection’ occur, then  $\xi_{orb} = 1$ . In Fig. 9 we give the time behaviour of  $\xi_{orb}$  for the clusters (c) and (d), only, because they keep a rather defined core on the whole duration of the simulation. In order to understand whether the tidal interaction with the galactic field influences appreciably the orbital decaying, it is worth comparing the clusters  $\xi_{orb}(t)$  evolution with that of two point-masses, moving within the same galactic potential with the same initial conditions of the clusters and experiencing the same df (Fig. 9), but free from tidal effects. Note that in the evaluation of the orbital energy of a cluster, the potential energy given by the interaction with the other is not taken into account; as we said in Sect. 3.1.1, the overall evolution of a cluster is not influenced appreciably by the presence of the other GC. Thus, to simplify the comparison, we considered the two point-masses as non-mutually interacting objects. Otherwise, we would have had to smooth the mutual gravitational force with a suitably variable smoothing radius, in order to simulate the variable



tidal distortion occurring for the clusters. Moreover, the mass of the point-masses is kept constant for consistency with the choice of constant clusters half-mass as a parameter in the df formula (see Appendix A).

We expected a different behaviour between the two cases, mainly because of the tidal interaction with the galaxy, that occurs only in the full  $N$ -body case and that, presumably, gives rise to a partial “thermalisation” of the orbital energy among the internal degrees of freedom, resulting in a further form of dissipation. This prediction is confirmed by the energy evolution, in the sense that the *rate* of dissipation is greater in the case of extended objects than for the two point-masses. The peaks shown by  $\xi_{orb}$  are due to the strong acceleration of the clusters CM during their close encounters (the mutual potential energy is not taken into account). To quantify the further frictional effect on the extended bodies, we followed the decay of the point-masses up to the time  $t_{dec}$  when  $\xi_{orb} \simeq 10^{-2}$ , i.e. when their orbit is confined to a region of size comparable with that of a typical GC. This happens at  $t_{dec} \sim 400$  for both the point-masses. On the other side, from Fig. 9, we can extrapolate a value of  $t_{dec}$  for the  $N$ -body systems assuming a constant energy decay rate, as  $t_{dec} \lesssim 180$  for the cluster (c) and  $t_{dec} \lesssim 280$  for the more compact but less massive cluster (d). Actually, these are overestimates, because the energy decay rate is generally increasing with time (see PCV and Capuzzo Dolcetta & Vicari 2005).

We must note, however, that the energy dissipation of the clusters depends on the particular way the df is evaluated. Indeed, as described in Appendix A, we used, in the Chandrasekhar formula, the kinematical quantities of the clusters CM that, due to the quick formation of large tails of stripped material, exhibits a very rapid decay towards the center, where the density and velocity dispersion of the galactic model have larger values than at the location of the main body (core) of the cluster. Actually, without an  $N$ -body self-consistent representation of the galaxy in which the satellite moves, the way to compute and assign the df deceleration to the bodies of a very extended object is not a trivial issue. It is difficult to model correctly the df changes induced by the cluster distortion and, maybe, even more difficult to take into account the gravitational feed-

back of the cluster *on* the galactic nuclear region, thus we were forced to do unavoidable simplifications. As explained in Appendix A, we assumed that the ‘global’ effect of the df is uniformly distributed to every GC star, and we evaluated it as if the cluster were concentrated in the CM position with the CM velocity. Even if questionable, this is a logical choice that would deserve a discussion, which is out of the purposes of this paper. In any case, we re-simulated (though with  $N = 10^4$ , for obvious computational convenience) the GCs evolution for models (c) and (d) (as individual systems in the galactic field), and with df computed by mean of the formula given by Eq. (A1) “centered” in the CD instead of the CM, and the comparison is shown in Fig. 9. The  $\xi_{orb}$  behaviour in these new simulations is flatter than that of the case with df evaluated at CM. The smaller effect of df is explained by that the CM is systematically closer to the galaxy center than the CD. Nevertheless the different amount of df does not modify qualitatively the global GC evolution at least within the simulated time. Note that a reliable estimate of the mass loss in the df-on-CD case cannot be achieved because the reduced number of particles ( $N = 10^4$ ) makes the 2-body relaxation time even shorter than the simulated time (see Eq. 6), thus affecting significantly the evolution with (spurious) collisional effects.

Considering the limited computational resources available, we chose to adopt an as more accurate as possible  $N$ -body representation of the cluster to study in detail the tidal disruption process, even if this forced us to employ an analytic single-component model for the galaxy, and so an analytic treatment of the df effect. However, the presence of velocity anisotropy for the field stars has to be taken into account, since it is important in altering the efficiency of the df as was proved by Binney (1977) in the axisymmetric case, then by PCV in the triaxial case and recently confirmed by the numerical simulations of Peñarrubia et al. (2004). Thus, we decided to use the PCV generalisation of the Chandrasekhar formula, with the self-consistent implementation of the analytic expression for the velocity dispersion tensor provided by the galactic model we adopted. Moreover, we took into account the change in the df caused by the non-uniform density of the field stars, through a suitable local estimate of the Coulomb log (see

Appendix A).

### 3.3. Tidal tails morphology

Tidal tails rapidly form around the clusters and follow closely their orbit (see Fig. 10). This tail-orbit alignment has been recently observed for the GC Palomar 5 (Odenkirchen et al. 2001, 2003) and also reproduced in various simulations (Charlton & Laguna 1995; Combes et al. 1999; Dehnen et al. 2004; Capuzzo Dolcetta et al. 2005). Since the velocity dispersion in the cluster outskirts (where most of the evaporated stars come from) is much lower than the cluster orbital velocity, it is not surprising that, there, stars move on orbits similar to that of the cluster itself, as clearly shown by Fig. 10. It can be also seen a significant spread of escaped stars around the apocenter of the cluster orbit. This because of the small differences among the velocities of the stars at the moment they leave the cluster become unimportant at the apocenter, where the orbital velocity is very low.

#### 3.3.1. Clumps and ripples formation

In our case, where GCs orbits are quasi-radial, centrifugal and Coriolis' forces are not important in determining the tails shape distortion investigated in CDM on a sample of less elongated orbits. Nevertheless, we do observe in our simulations the presence of stellar overdensities along the tidal tails, similar to those seen around the mentioned Pal 5 and in the simulations in CDM.

The cluster (b) is plotted at various times close to the first passage at the rightmost apocenter, in Figs 11–12. A “ripple” starts to form around  $x = 3.1$  at  $t = 8.6$ , as a ‘wave-like’ overdensity. Then, the cluster travels for a while across and then above the formed ripple ( $t = 9.2$ – $9.7$ ), before reaching its apocenter. It can be also seen that at  $t = 10.3$  (Fig. 12) another ripple forms again around  $x = 4.1$ , while at  $t = 9.7$  the one previously formed begins to move inward giving rise, at  $t = 10.5$ , to a clump—an overdensity with a roughly spherical shape—around  $x = 3.2$ . All these plots are projections on the  $xy$  plane, however all the structures are almost aligned along the orbit around which (i.e. around the  $x$ -axis) they show a roughly cylindrical symmetry; as an example the ripples are, actually, thin discoidal structures. This can be seen in the available 3-d

animations (see below).

To explain the overdensities found in the tails of the mentioned Palomar 5, Dehnen et al. (2004) raised an hypothesis stating that clumps could be due to the effect of the interaction with Galactic substructures (like giant molecular clouds, spiral arms, dark-matter sub-halos or massive compact halo objects). Basically, their opinion is that small-scale overdensities like clumps can only be built up by the tidal interaction with fluctuations on relatively small-scale of the external gravitational field. On the contrary, the results shown here seem to confirm the findings of CDM, in the sense that in the absence of any small-scale substructure in the overall potential clumps form too, thus suggesting that a further mechanism is at work.

Analysing the local velocity measured along the orbital path and the energy of the stars in the cluster field, we can affirm that both clumps and the apocenter ripple are not gravitationally-bound aggregates but, rather, overdensities due to the local deceleration of the stellar motion, as already verified in CDM and in Di Matteo et al. (2005). On the contrary, where the velocity increases towards the direction of the stellar mean motion along the tails, the tails tend to rarefy and an underdensity occurs. The metaphor of the “motorway traffic jam” mechanism used in Dehnen et al. (2004) is effective here, as can be seen in Fig. 13. The cause of the overdensity is the strong deceleration of the stellar flux immediately on the left of the ripple location (around  $x = 3.25$ ). Note that inside the cluster the profile of  $\langle v_x \rangle$  is nearly flat as expected for a bound (almost rigid) object, while in the ripple region it exhibits a non-zero gradient.

It is interesting to compare a configuration like those shown in Fig. 12 at  $t = 10.3$  and  $t = 10.5$ , with the ‘arcs’ of material observed around the spectacular shell galaxy NGC 3923 (Fort et al. 1986; Pence 1986) as well as with the results of the simulations in Hernquist & Quinn (1987, 1988); Heisler & White (1990) and Bournaud et al. (2004). Although different scenarios and length-scale are involved, the qualitative features of the debris produced by the tidal interaction of a compact and smaller object with a larger density distribution, are rather similar to what we found in this paper. In particular, sharp-edged structures in form of ‘ripples’ or ‘arcs’ are formed when the

satellite moves on a very elongated orbit in a regular potential generated by a much more massive and larger object.

To conclude this Section, we give the web address <http://inaf.cineca.it/KP/kp4.html> where the reader can get animations regarding some parts of the simulation A. The first animation refers to the whole simulation and one can see how the least compact GCs get destroyed. The second animation is a zoom around the apogalacticon, that corresponds to the Figures 11–12 of the sub-structures formation.

#### 4. Conclusions

In this first of a series of papers we investigated the effects of the central galactic environment on the structure of globular clusters decayed in the inner region because of dynamical friction. Our main concern is to answer the following questions: i) to what extent are clusters able to survive the strong tidal interaction with the galaxy? ii) do they keep their compact structure long enough to permit dynamical friction to dissipate completely their orbital energy? iii) what are the effects of close encounters and collisions between clusters?

The main conclusions of our work can be summarized as follows.

Sufficiently compact clusters (initial King concentration parameter  $c \geq 1.2$ ) can survive the tidal interaction with the external fields for, at least, the duration of our simulations, i.e. for 8 passages across the galactic center ( $t \simeq 40t_b$ , being  $t_b$  the galaxy core crossing time), while those with  $c = 0.8$ – $0.9$  are almost disintegrated after only 2–3 passages ( $\sim 10$ – $15t_b$ ). The mass loss from the clusters as a function of time follows an exponential law  $\sim e^{-t/\tau}$  with  $\tau$  up to  $\sim 70t_b$  for the most compact cluster ( $c = 1.3$ ). Even if still without a high statistical reliability, we found a correlation between the mass loss time-scale and the concentration parameter that can be quantified as  $\tau \simeq 14c^{6.1}$ . This means that a GC with an initial  $c \gtrsim 1.6$  keeps bound a substantial amount of its mass up to  $t \simeq 300t_b$ , i.e. up to the complete orbital decaying.

During their evolution, the survived clusters maintain the initial King profile in the inner region, with a *decreasing* concentration and a *constant* central velocity dispersion. A small degree of

mass segregation occurs at the end of the simulations: the average stellar mass in the central clusters region increases of about 10% of the initial value, but the fluctuations are even larger. The very low level of mass segregation is not surprising, for the half-mass relaxation time is  $\sim 6$  times longer than the simulated time.

With regard to the orbital decay, we found that the tidal interaction with the field gives rise to a dissipation of the orbital energy with a rate comparable to that given by the df, when this is evaluated at the cluster CM. However, even when the CD is used instead of this latter, we found that the tidal interaction provides a further important mechanism of orbital decaying besides dynamical friction (included in our simulations). This is important for the validity of the nucleus accretion model according to which the nuclear region receives a large amount of mass in form of clusters that have lost their orbital energy (Capuzzo Dolcetta 1993; Capuzzo Dolcetta & Vicari 2005).

Another relevant finding of this work is that, in the cases considered here, the tidal interaction between the two clusters, even during face-on collisions, produces negligible effects on both their internal evolution and their orbital evolution (at least for  $t < 40t_b$ ), confirming the estimates done according to the impulse approximation.

All these results indicate that sufficiently massive and compact clusters can survive the disruptive effect due to the strong tidal forces exerted by the central environment. Dynamical friction *and* tidal dissipation are then able to brake many globular clusters *before* they are disintegrated, so to allow the formation of a dense and massive super-cluster resulting from merging events among clusters. The simulations shown here did not achieve the final merging stage between the objects, because of the limits in the computational resources. In a forthcoming paper, we will present results of a new series of simulations directly regarding the merging among clusters. Indeed, the importance of the present work is also to get physically reliable and realistic initial conditions from which the simulations of the final merging process will start.

A further result of this work concerns the formation and structure of tidal tails. Tidal tails form rather quickly, with a clear tendency to align along the orbital path. They exhibit complex morphology, with the presence of clumps and ‘rip-

ples' as those observed around globular clusters and shell galaxies, too. Such overdensities are not gravitationally bound aggregates but, rather, their formation seems to have a kinematical origin, being connected to the deceleration of the stellar 'flux' motion along the tails.

## 5. Acknowledgements

The main computational resources employed for this work were provided by CINECA (<http://www.cineca.it>) and INAF (<http://inaf.cineca.it>) agreement under the *Key-Project* grant *inarm033*. Part of this work was also supported by MIUR (Ministero dell'Istruzione dell'Università e della Ricerca) under the *PRIN 2001* funding program (grant 2001028897\_005).

## A. Treatment of the dynamical friction

The effect of braking due to df on globular clusters was followed by the same approach used in PCV. The classic formula developed by Chandrasekhar (1943) for the df deceleration term has been extended by PCV to the triaxial case, in partial analogy with the (Binney 1977) extension to the axisymmetric case, obtaining:

$$\mathbf{a}_{df} = -\gamma_1 V_1 \hat{\mathbf{e}}_1 - \gamma_2 V_2 \hat{\mathbf{e}}_2 - \gamma_3 V_3 \hat{\mathbf{e}}_3 \quad (\text{A1})$$

where  $\hat{\mathbf{e}}_i$  ( $i = 1, 2, 3$ ) are the eigenvectors of the velocity dispersion tensor of the galaxy stars and  $V_i$  is the component of the velocity of the baricenter of the GC along the  $\hat{\mathbf{e}}_i$  axis. The coefficients  $\gamma_i$  are (see PCV):

$$\begin{aligned} \gamma_i = & \frac{2\sqrt{2\pi}\rho(\mathbf{r})G^2M\ln\Lambda}{\sigma_1^3} \times \\ & \times \int_0^\infty \exp\left(-\sum_{k=1}^3 \frac{V_k/2\sigma_k^2}{\epsilon_k^2 + u}\right) \times \\ & \times (\epsilon_i^2 + u)^{-1} \left[ \sum_{k=1}^3 (\epsilon_k^2 + u) \right]^{-1/2} du \end{aligned} \quad (\text{A2})$$

where:  $\rho(\mathbf{r})$  is the mass density of background stars,  $\ln\Lambda$  is the Coulomb's logarithm,  $M$  is the mass of the test object,  $G$  is the gravitational constant,  $\sigma_i$  is the eigenvalue, corresponding to  $\hat{\mathbf{e}}_i$ , of the velocity dispersion tensor  $\sigma_{ij}$  evaluated in  $\mathbf{r}$ , and  $\epsilon_i$  is the ratio between  $\sigma_i$  and the greatest eigenvalue, set as  $\sigma_1$ .

The velocity dispersion was computed and presented by Merritt (1980) for the Schwarzschild ellipsoid, both in the case of a rotating and a non-rotating model. In this paper we considered just the non-rotating model.

For computational convenience, the Merritt's data were fitted obtaining three analytical expressions for the eigenvalues  $\sigma_3 < \sigma_2 < \sigma_1$  at  $\tilde{r} \equiv |\mathbf{r}|/r_b$ :

$$\begin{aligned} \sigma_1^2 &= 3.1e^{-\tilde{r}/9.2} \\ \sigma_2^2 &= \frac{2.9}{1 + 0.43\tilde{r}^{1.60}} \\ \sigma_3^2 &= \frac{2}{1 + 0.44\tilde{r}^{1.7}} \end{aligned} \quad (\text{A3})$$

(expressed in unit of  $GM_b/r_b$ ). Analogously, the following fitting formulas for the Euler angles giving the orientation of the local reference frame where  $\sigma_{ij}$  is diagonal were determined:

$$\begin{aligned} \alpha &= \pi/2 + \frac{0.2\tilde{r}^{2.3}}{1 + 0.2\tilde{r}^{2.3}} [\arccos(\tilde{z}/\tilde{r}) - \pi/2] \\ \beta &= \pi/2 + \frac{0.2\tilde{r}^{2.25}}{1 + 0.2\tilde{r}^{2.25}} \arcsin\left(\frac{\tilde{y}}{\sqrt{\tilde{x}^2 + \tilde{y}^2}}\right) \\ \gamma &= \frac{0.8\tilde{r}^3}{1 + 0.8\tilde{r}^3} \arcsin\left(\frac{\tilde{y}}{\sqrt{\tilde{x}^2 + \tilde{y}^2}}\right) \end{aligned} \quad (\text{A4})$$

The fitting formulas A3 and A4 are a slight improvement of those reported in PCV.

Given  $b_M$  and  $b_m$  respectively, the maximum and the minimum impact parameter of the test object with field stars, we adopted a variable and local Coulomb's logarithm  $\ln\Lambda = \ln(b_M/b_m)$  assuming  $b_m = GM_{1/2}/\sigma^2(\mathbf{r})$ , where  $\sigma^2(\mathbf{r}) = \sigma_1^2 + \sigma_2^2 + \sigma_3^2$  and  $M_{1/2} = M/2$  is the cluster initial half-mass. Indeed, since the GC is not a point-mass, the df is made less efficient by the 'weakening' of the encounters with impact

parameters smaller than the size of the object itself, assumed as the half-mass radius (see e.g. Binney & Tremaine 1987). Of course, this reasoning is based on the hypothesis that at least the core of the cluster survives to the tidal stress so to make it to be able to continue acting on a compact object with mass  $\sim M_{1/2}$ , throughout the whole simulated time. Our choice of letting  $b_M = 10r_b$  seems quite adequate to our quasi-radial orbits, noting that the stellar density at a distance  $r > 10r_b$  from the galactic center falls below  $10^{-3}$  times the central value. Choices of  $b_M$  as function of the galactocentric distance, like for instance  $b_M = r$  (Hashimoto et al. 2003), are of not straightforward use in our cases.

Finally, the acceleration given by Eq. (A1) is evaluated either at the CM or at the CD position of the cluster and then added to the accelerations of every particle of the cluster.

## B. The $N$ -body approach

The simulations have been performed by means of the code ‘ATD’ (Miocchi & Capuzzo Dolcetta 2002). It is a parallel *tree-code* that follows, in part, the Barnes & Hut (1986) algorithm. For the potential due to distant ‘particles’ it uses a multipolar expansion truncated at the quadrupole moment and has been parallelized to run on high performance computers via MPI routines, employing an original parallelization approach. A good resolution in the evaluation of the total gravitational force acting on each star of the cluster is achieved by a direct summation of the contribution given by neighbours. To avoid instability in the time-integration, the  $1/r$  gravitational potential has been smoothed by using a continuous  $\beta$ -spline function for  $r < \epsilon$ , such to give an exactly Newtonian potential for  $r > \epsilon$  (Hernquist & Katz 1989) and a force that vanishes as  $r$  for  $r \rightarrow 0$ . The time-integration of the ‘particles’ trajectories is performed according to the leap-frog algorithm. This latter uses individual and variable time-steps according to the block-time scheme (Aarseth 1985; Hernquist & Katz 1989), in addition with corrections we implemented in order to keep the same order of approximation also during the time-step change. Denoting by  $t_c$  the minimum core-crossing time of our simulated clusters, the maximum allowed time-step is  $\Delta t_{\max} = 0.01t_c$ , while the minimum is  $\Delta t_{\min} = \Delta t_{\max}/2^{10}$ , thus fastest particles may have a time-step as small as  $\sim 10^{-5}t_c$ . To choose the time-step of the  $i$ -th particle we found that the best compromise between accuracy and speed in the time-integration is via the formula:  $\Delta t_i = 0.05 \times \min\{(d_i/a_i)^{1/2}, d_i/v_i\}$ , where  $v_i$  is the velocity of the particle relative to its first neighbour (or to the CM of its closest box),  $d_i$  its distance from the first neighbour and  $a_i$  the modulus of the total acceleration of the  $i$ -th particle itself.

In all the runs the softening length  $\epsilon$  is set to  $10^{-5}r_b$  (i.e.  $2 \times 10^{-3}$  pc if  $r_b = 200$  pc), so to have  $(\epsilon^3/GM)^{1/2} \sim \Delta t_{\min}$ . This is a minimal condition to ensure that the level of accuracy in the forces evaluation agrees with the accuracy in the time-integration scheme. Note that such an  $\epsilon$  is much smaller than the typical interparticle distance so to keep the overall correct Newtonian behaviour. For  $N$  lower than the real number of stars, as in our case, the choice of the gravitational smoothing radius is a matter of compromise between the need for maintaining the Newtonian behaviour (the smaller is  $\epsilon$  the more correct is the force evaluation) and the need for avoiding a spurious increase of collisionality (the larger is  $\epsilon$  the closer is the model relaxation time to the real one). As a matter of fact, the results discussed in Sect. 3.1.3 suggest that  $\epsilon$  is large enough not to introduce fictitious collisional effects.

## REFERENCES

- Aarseth, S.J. 1985, in 'Multiple time scales', Acad. Press, 378
- Aguilar, L., Hut, P., & Ostriker, J.P. 1988, ApJ, 335, 720
- Ashman, K.M., & Zepf, S.E. 1997, Globular Cluster Systems (Cambridge: Cambridge Univ. Press)
- Baumgardt, H., & Makino, J. 2003, MNRAS, 340, 227
- Baumgardt, H., Makino, J., Hut, P., McMillan, S., & Portegies Zwart, S. 2003, ApJ, 589, L25
- Barnes, J., & Hut, P. 1986, Nature, 324, 446
- Bertola, F., Vietri, M., & Zeilinger, W.W. 1991, ApJ, 374, L13
- Binney J. 1977, MNRAS, 181, 735
- Binney, J., & Tremaine, S. 1987, Galactic Dynamics, Princeton Univ. Press
- Bournaud, F., Duc, P.A., Amram, P., Combes, F., & Gach, J.L. 2004, A&A, 425, 813
- Capuzzo Dolcetta, R. 1993, ApJ, 415, 616
- Capuzzo Dolcetta, R., Di Matteo, P., & Miocchi, P. 2005, AJ, 129, 1906
- Capuzzo Dolcetta, R., & Tesseri, A. 1997, MNRAS, 292, 808
- Capuzzo Dolcetta, R., & Tesseri, A. 1999, MNRAS, 308, 961
- Capuzzo Dolcetta, R., & Vicari, A. 2005, MNRAS, 356, 899
- Casertano, S., & Hut, P. 1985, ApJ, 298, 80
- Chandrasekhar, S. 1943, ApJ, 97, 255
- Charlton, J.C., & Laguna, P. 1995, ApJ, 444, 193
- Colpi, M., Mayer, L., & Governato, F., 1999, ApJ, 525, 720
- Combes, F., Leon, S., & Meylan, G. 1999, A&A, 352, 149
- Davidge, T. J., & van den Bergh, S. 2005, PASP, 117, 589
- Davies, R. L. , Kuntschner, H. , Emsellem, E., Bacon, R., Bureau, M., Carollo, C.M., Copin, Y., Miller, B.W., Monnet, G., Peletier, R.F., Verolme, E.K., & de Zeeuw, P.T. 2001, ApJ, 548/1, L33
- Dehnen, W., Odenkirchen, M., Grebel, E. K., & Rix, H. W. 2004, AJ, 127, 2753.
- de Grijs, R., Wilkinson M. I. & Tadhunter, C. N. 2005, MNRAS, 361, 311
- de Zeeuw, T., & Merritt, D. 1983, ApJ, 267, 571
- Di Matteo, P., Capuzzo Dolcetta, R., & Miocchi, P. 2005, Cel. Mech. & Dyn. Astron., 91, 59
- Dirsch, B., Schubert, Y., & Richtler, T. 2005, A&A, 433, 43
- Elson, R. A. W., Fall, S. M., & Freeman, K.C. 1987, ApJ, 323, 54
- Fall, S. M.; Rees, M. J. 1985, ApJ, .298, 18
- Fellhauer, M., & Kroupa, P. 2002, MNRAS, 330, 642
- Forbes, D. A., Strader, J., & Brodie, J. P. 2004, AJ, 127, 3394
- Fort, B.P., Prieur, J.P., Carter, D., Meatheringham, S., & Vigroux, L. 1986, ApJ, 306, 110
- Fritze-v. Alvensleben, U. 1999, A&A, 342, L25
- Fusi Pecci, F., Bellazzini, M., Buzzoni, A., De Simone, E., Federici, L. & Galletti, S. 2005, AJ, 130, 554
- Giersz, M., & Heggie, D.C. 1994, MNRAS, 268, 257
- Gnedin, O.Y., & Ostriker, J.P. 1997, ApJ, 474, 223
- Gnedin, O.Y., Lee, H.M., & Ostriker, J.P. 1999, ApJ, 522, 935
- Gomez, M., Richtler, T., Infante, L., & Drenkhahn, G. 2001, A&A, 371, 875
- Gomez, M., & Richtler, T. 2004, A&A, 415, 499

- Goodwin, S. P. 1998, MNRAS, 294, 47
- Grillmair, C.J., Freeman, K.C., Irwin, M., & Quinn, P.J. 1995, AJ, 109, 2553
- Harris, G. L. H., Harris, W. E., & Geisler, D. 2004, AJ, 128, 723
- Harris, G. L. H., Geisler, D., Harris, W. E., Schmidt, B. P., Hesser, J. E., Reid, M., Milne, M., Hulme, S. C., & Kidd, T. T. 2004, AJ, 128, 712
- Harris, W.E., Whitmore, B.C., Karakla, D., Okon, W., Baum, W. A., Hanes, D.A. & Kavelaars, J. J. 2006, ApJ, 636, 90
- Harris, W.E. & Pudritz, R.E. 1994, ApJ, 429, 177
- Hashimoto, Y., Funato, Y., & Makino, J. 2003, ApJ, 582, 196
- Heisler, J., & White, S. 1990, MNRAS, 243, 199
- Hernquist, L., & Katz, N. 1989, ApJS, 70, 419
- Hernquist, L., & Quinn, P.J. 1987, ApJ, 312, 1
- Hernquist, L., & Quinn, P.J. 1988, ApJ, 331, 682
- Huxor, A.P., Tanvir, N.R., Irwin, M.J., Ibata, R., Collett, J.L., Ferguson, A.M.N., Bridges, T., & Lewis, G.F. 2005, MNRAS, 360, 1007
- Ideta, M., & Makino, J. 2004, ApJ, 616, L107
- King, I.R. 1966, AJ, 71, 64
- Kravtsov, A.V. & Gnedin, O.Y. 2005, ApJ, 623, 650
- Kundu, A., Whitmore, B.C., Sparks, W.B., Macchetto, F.D., Zepf, S.E., & Ashman, K.M. 1999, ApJ, 513, 733
- Kundu, A., Morton, D. 2004, AAS Meeting, 205, 85.01
- Lee, K.H., Lee, H.M., Fahlman, G.G., & Lee, M.G. 2003, AJ, 126, 815
- Lehmann, I., & Scholz, R.D. 1997, A&A, 320, 776
- Leon, S., Meylan, G., & Combes, F. 2000, A&A, 359, 907
- Matthews, L.D., & de Grijs, R. 2004, AJ, 128/1, 137
- McGlynn, T.A. 1984, ApJ, 281, 13
- Mc Laughlin D.E., Harris W.E., Hanes D.A. 1994, ApJ, 422, 486
- Meylan, G., & Heggie, D.C. 1997, A&A Rev., 8, 1
- Merritt, D. 1980, ApJS, 43, 435
- Miocchi, P., & Capuzzo Dolcetta, R. 2002, A&A, 382, 758
- Murali, C., & Weinberg, M., D. 1997a, MNRAS, 288, 749
- Murali, C., & Weinberg, M., D. 1997b, MNRAS, 288, 767
- Nordquist, H. K., Klinger, R. J., Laguna, P., & Charlton, J.C. 1999, MNRAS, 304, 288
- Odenkirchen, M., Grebel, E, K., Dehnen, W, Rix, H. W., Yanny, B., Newberg, H. J., Rockosi, C. M., Martínez-Delgado, D., Brinkmann, J., & Pier, J. R. 2003, AJ, 126, 2385
- Odenkirchen, M. et al. 2001, ApJ, 548, L165
- Olsen, K. A. G., Miller, B. W., Suntzeff, N. B., Schommer, R. A., & Bright, J. 2004, AJ, 127, 2674
- Ostriker, J.P., Binney, J., & Saha, P. 1989, MNRAS, 241, 849
- Peñarrubia, J., Kroupa, P., & Boily, C.M. 2002, MNRAS, 333, 779
- Peñarrubia, J., Just, J., & Kroupa, P. 2004, MNRAS, 349, 747
- Pence, W.D. 1986, ApJ, 310, 597
- Pesce, E., Capuzzo Dolcetta, R., & Vietri, M. 1992, MNRAS, 254, 466
- Schwarzschild, M. 1979, ApJ, 232, 236
- Siegel, M. H., Majewski, S. R., Cudworth, K. M., & Takamiya, M. 2001, AJ, 121, 935
- Spitzer, L. Jr., & Chevalier, R.A. 1973, ApJ, 183, 565
- Spitzer, L. Jr., & Shull, J. M. 1975, ApJ, 201, 773



- Spitzer, L. Jr. 1987, *Dynamical Evolution of Globular Clusters* (Princeton: Princeton University Press)
- Statler, T.S., Emsellem, E., Peletier, R. F., & Bacon, R. 2004, *MNRAS*, 353, 1
- Steinmetz, M., & White, S.D.M. 1997, *MNRAS*, 288, 545
- Testa, V., Zaggia, S. R., Andreon, S., Longo, G., Scaramella, R., Djorgovski, S. G., & de Carvalho, R. 2000, *A&A*, 356, 127
- Tremaine, S., Ostriker, J.P., & Spitzer, L. Jr. 1975, *ApJ*, 196, 407
- van Albada, T.S. 1982, *MNRAS*, 201, 939
- van den Bosch, F. C., Lewis, G.F., Lake, G., & Stadel, J. 1999, *ApJ*, 515, 50
- Vesperini E. 2001, *MNRAS*, 322, 247
- Vietri, M., & Pesce, E. 1995, *ApJ*, 442, 618
- Wagner, S.J., Bender, R., & Moellenhoff, C. 1988, *A&A*, 195, L5
- Zepf, S. E., Bergond, G., Romanowsky, A. J., Rhode, K. L. & Sharples, R. M. 2004, *AAS Meeting*, 205, 31.04

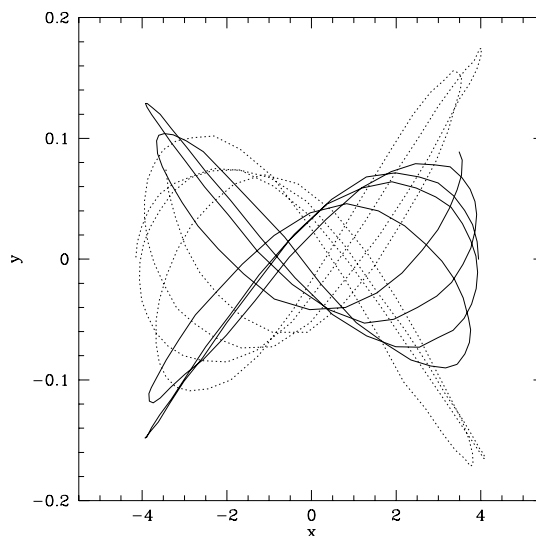


Fig. 1.— Center-of-density trajectories on the  $xy$  plane, for cluster (c) (dotted line) and (d) (solid line) in the Simulation B.

TABLE 1  
CLUSTERS INITIAL PARAMETERS.

cluster model	$M \times 10^3$	$r_t$	$c$	$r_c \times 10^2$	$t_c \times 10^2$	$\sigma$	Simulation
<b>a</b>	6.7	0.47	0.8	7	23	0.13	<b>A, C</b>
<b>b</b>	5	0.36	0.9	4.5	13	0.13	<b>A</b>
<b>c</b>	6.7	0.49	1.2	2.7	5.4	0.14	<b>B</b>
<b>d</b>	5	0.38	1.3	1.9	3.7	0.14	<b>B</b>

NOTE.—Parameters list for the initial cluster models. Masses, lengths and time are in unit of  $M_b$ ,  $r_b$  and  $t_b$  respectively.

TABLE 2  
PARAMETERS FOR THE MASS LOSS FITS.

cluster model	$a_E$	$\tau_E$	$a_{0.1}$	$\tau_{0.1}$	$a_1$	$\tau_1$
<b>a</b> (sim. A)	3.8	3.2	0.75	35	0.51	15
<b>b</b>	1.9	9.7	0.91	33	1.2	14
<b>c</b>	0.77	46	0.83	56	0.72	45
<b>d</b>	0.89	65	0.88	74	0.79	69

NOTE.—Parameters of the mass loss evolution  $1 - ae^{-t/\tau}$ , according to the criteria based on: the total internal energy ( $a_E, \tau_E$ ), the density contrast of 10% ( $a_{0.1}, \tau_{0.1}$ ) and 100% ( $a_1, \tau_1$ ). Time is in unit of  $t_b$ .

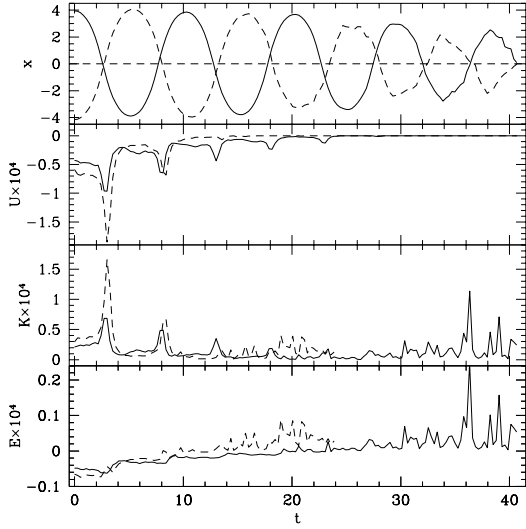


Fig. 2.— From top to bottom: CD motion along  $x$ -axis for the pair of (looser) clusters (a) and (b) in the simulation A; time behaviour of the potential ( $U$ ), kinetic ( $K$ ) and total ( $E$ ) internal energy (solid line: model (b) , dashed: model (a) ). Energies are evaluated in the center-of-density frame and they are concerned only with the stars in the sphere with radius equal to the initial King radius of each cluster. For the loosest cluster (a) the energy is plotted up to  $t \sim 24$  because, afterwards, it is almost destroyed. The case of the cluster (a) evolving alone in the simulation C showed no appreciable differences in respect to the simulation A.

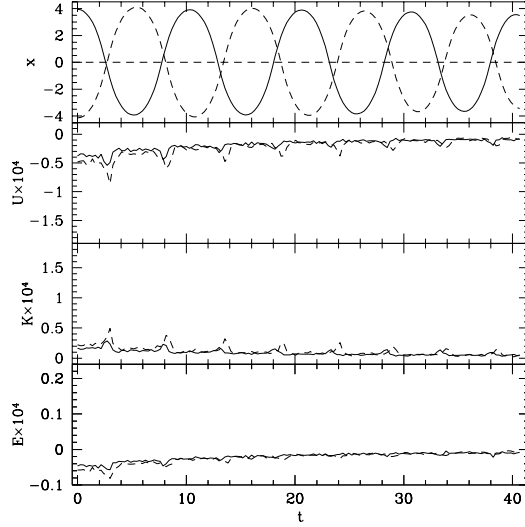


Fig. 3.— From top to bottom: CD motion along  $x$ -axis for the pair of the more compact clusters ((c) and (d) ) in the simulation B, time behaviour of the potential, kinetic and total internal energy (solid line: model (d) , dashed: model (c) ). Energies are evaluated as in Fig. 2.

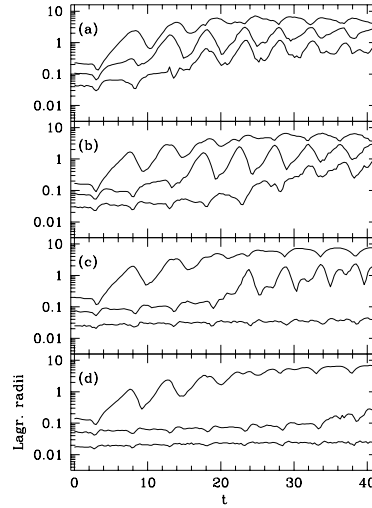


Fig. 4.— Lagrangian radii evolution for the 4 cluster models (as labelled). In each panel, the radii of 10, 50 and 90% of the total mass are shown.

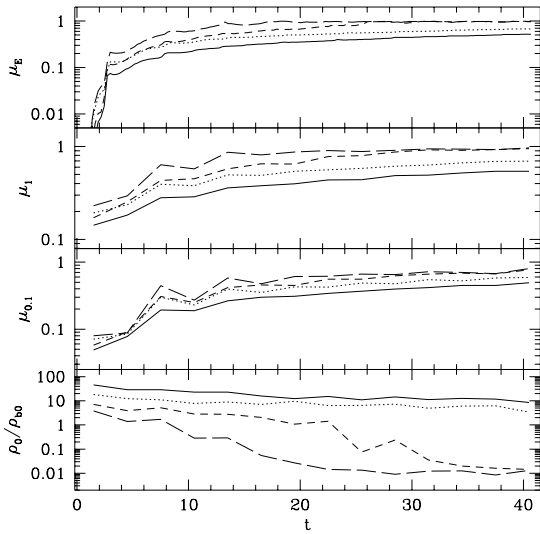


Fig. 5.— Different evaluations of the time evolution of the fraction of mass lost from the clusters (see text). Bottom panel: time evolution of the central density normalized to the galaxy central density. Solid line: model (d) , dotted: (c) , short dashed: (b) , long dashed: cluster (a) in the simulation A. The curves are time-averaged over  $3t_b$ .

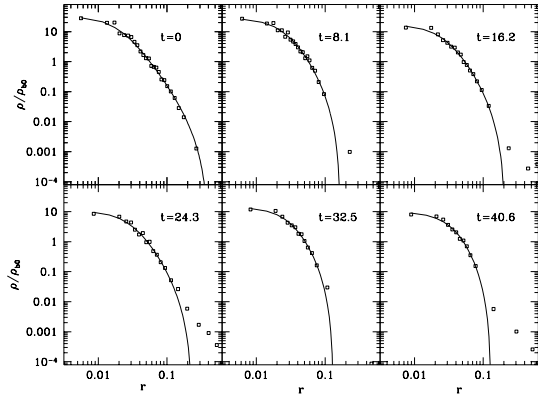


Fig. 6.— Cluster density profile (squares), for the model (d) at various times. The sampled spherical shells have width such to contain a constant number of particles. The density is normalized to the galaxy central density. The solid curve is the best King model fit.

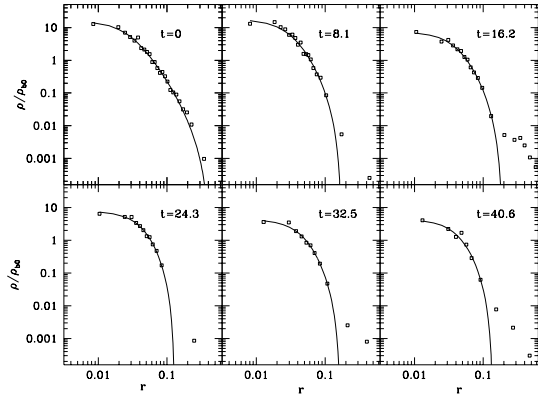


Fig. 7.— As in Fig. 6 for the cluster (c) .

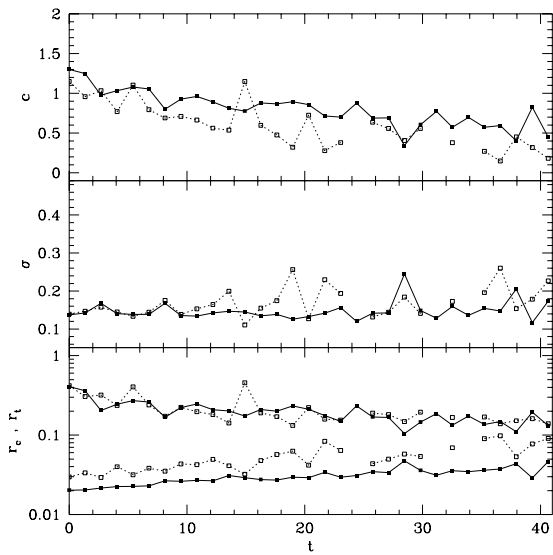


Fig. 8.— From top to bottom: evolution of the concentration parameter,  $c$ , of the central velocity dispersion,  $\sigma$ , and of the King and limiting radii ( $r_c$ ,  $r_t$ ) for the best King model fits to clusters (c) (open squares, dotted line) and (d) (solid squares and solid line).

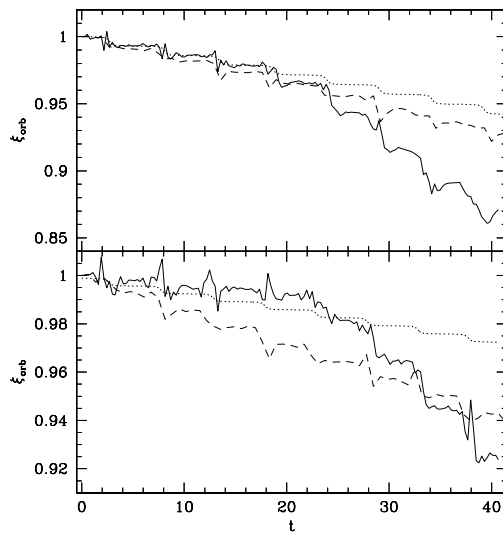


Fig. 9.— Time behaviour of the fraction of orbital energy kept, at time  $t$ , by the clusters in the simulation B (solid line) and by the corresponding point-mass (dotted line). Upper panel: cluster (c) ; lower panel: cluster (d) . For comparison, the case with the  $df$  evaluated at the cluster CD by mean of the ‘reduced’ simulations (see text) is also plotted (dashed line).

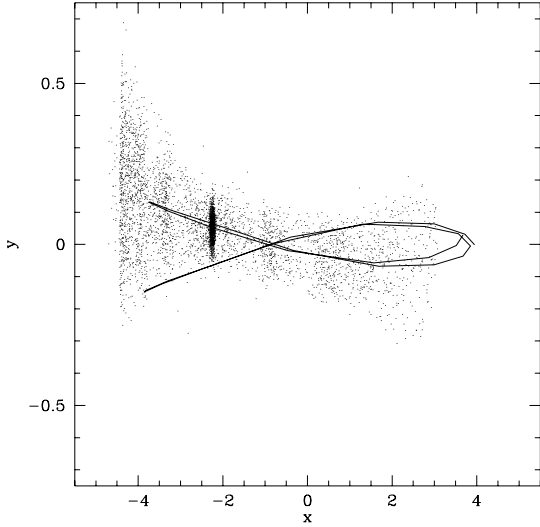


Fig. 10.— Configuration of cluster (b) at  $t = 17$ . The projected trajectory of its center-of-density motion is also plotted. The  $y$ -axis scale is expanded to show better the alignment between the cluster orbit and the tails.

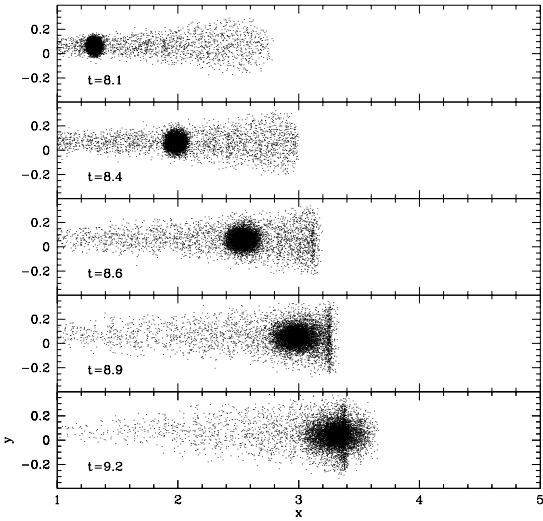


Fig. 11.— Cluster (b) is sketched at various times (as labelled) before the first passage to the right-most apocenter (galactic center is at  $x = 0$ ).

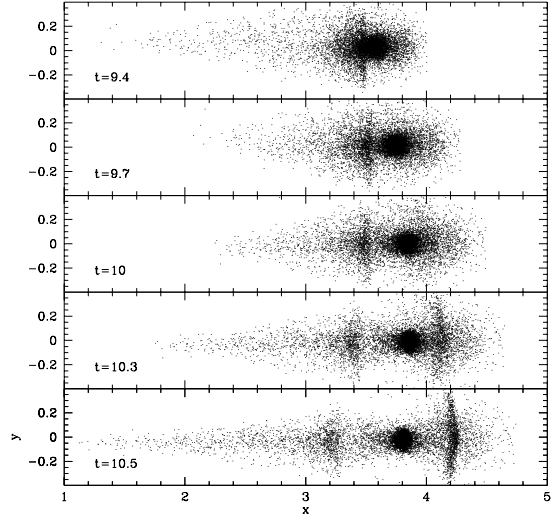


Fig. 12.— Continuation of Fig. 11 for the same cluster (b); the apocenter is reached at  $t \sim 10$ .

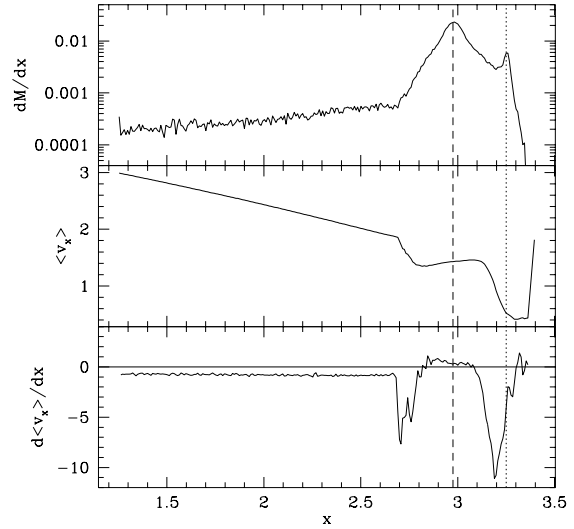


Fig. 13.— The plots refer to the cluster shown in Fig. 11 at  $t = 8.9$ . Upper panel: linear density as measured along  $x$ -axis. Middle panel: averaged stellar velocity component ( $\langle v_x \rangle$ ) along  $x$ . Lower: spatial derivative of  $\langle v_x \rangle$  (the horizontal line indicates the zero value). The position of the GC and of the ‘ripple’ are marked, respectively, by the dashed and dotted lines (galactic center is at  $x = 0$ ).

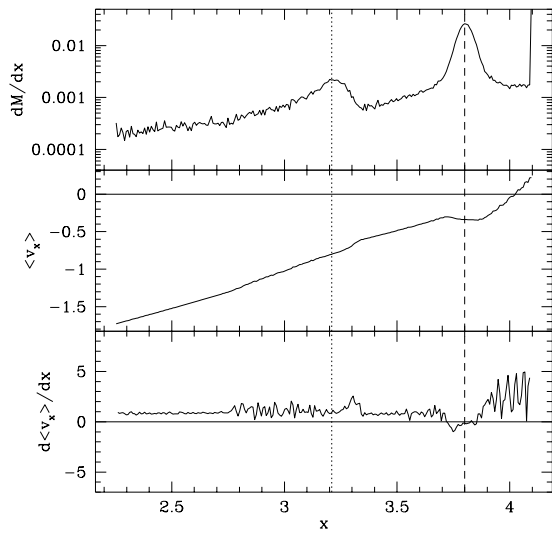


Fig. 14.— As in Fig. 13 but referring to the time  $t = 10.5$ . The position of the GC is marked by the dashed line, while the ‘clump’ is at the dotted one.